Amacrine Cell Subtypes Differ in Their Intrinsic Neurite Growth Capacity

Noelia J. Kunzevitzky,[1–4] Kevin T. Willeford,[2,5] William J. Feuer,[2] Monica V. Almeida,[2] and Jeffrey L. Goldberg[1–5]

[1]Shiley Eye Center, University of California–San Diego, La Jolla, California
[2]Bascom Palmer Eye Institute, Miami, Florida
[3]Graduate Program in Molecular Cell and Developmental Biology, University of Miami Miller School of Medicine, Miami, Florida
[4]Interdisciplinary Stem Cell Institute, University of Miami Miller School of Medicine, Miami, Florida
[5]Undergraduate Program in Neuroscience, University of Miami, Miami, Florida

Correspondence: Jeffrey L. Goldberg, University of California–San Diego, Shiley Eye Center, 9415 Campus Point Drive #0946, La Jolla, CA 92093-0946; jlgoldberg@ucsd.edu.

Submitted: June 27, 2013
Accepted: September 23, 2013

Citation: Kunzevitzky NJ, Willeford KT, Feuer WJ, Almeida MV, Goldberg JL. Amacrine cell subtypes differ in their intrinsic neurite growth capacity. *Invest Ophthalmol Vis Sci*. 2013;54:7603–7613. DOI:10.1167/iovs.13-12691

Purpose. Amacrine cell neurite patterning has been extensively studied in vivo, and more than 30 subpopulations with varied morphologies have been identified in the mammalian retina. It is not known, however, whether the complex amacrine cell morphology is determined intrinsically, is signaled by extrinsic cues, or both.

Methods. Here we purified rat amacrine cell subpopulations away from their retinal neighbors and glial-derived factors to ask questions about their intrinsic neurite growth ability. In defined medium strongly trophic for amacrine cells in vitro, we characterized survival and neurite growth of amacrine cell subpopulations defined by expression of specific markers.

Results. We found that a series of amacrine cell subtype markers are developmentally regulated, turning on through early postnatal development. Subtype marker expression was observed in similar fractions of cultured amacrine cells as was observed in vivo, and was maintained with time in culture. Overall, amacrine cell neurite growth followed principles very similar to those in postnatal retinal ganglion cells, but embryonic retinal ganglion cells demonstrated different features, relating to their rapid axon growth. Surprisingly, the three subpopulations of amacrine cells studied in vitro recapitulated quantitatively and qualitatively the varied morphologies they have in vivo.

Conclusions. Our data suggest that cultured amacrine cells maintain intrinsic fidelity to their identified in vivo subtypes, and furthermore, that cell-autonomous, intrinsic factors contribute to the regulation of neurite patterning.

Keywords: amacrine cells, retinal development, neurite patterning, intrinsic neurite growth

Amacrine cells are a heterogeneous group of retinal interneurons with a widely varied and complex neurite patterning. There are more than 30 morphologic subtypes described in the mammalian retina,[1–3] which range from having few to multiple neurites that may include short or long, axon-like processes, or thin or bushy dendritic-like trees. Additional criteria for amacrine cell subtype classification include the synaptic laminae of their neurites in the inner plexiform layer, the neurotransmitters they secrete, and the specific markers they express.

Despite these myriad morphologies, little is known about the factors that determine amacrine cells' morphological patterning. Previous studies have suggested the importance of extrinsic signals contributing to neural patterning in the retina,[4–6] drawn from the extensive characterization of amacrine cell morphology in vivo.[2,7] Drawing conclusions about any contribution of intrinsic or cell-autonomous contributions to neurite patterning, however, is naturally limited by the lack of ex vivo studies.

The use of in vitro cultures may help elucidate whether there is any role for intrinsic regulation of neurite growth. For example, purified cultures were previously used to demonstrate developmental regulation of intrinsic axon growth ability in retinal ganglion cells (RGCs).[8] Here we take advantage of our ability to highly purify retinal amacrine cells to ask, do purified amacrine cells in vitro recapitulate the neurite grown patterns that they have in vivo? These data argue for at least a contribution of intrinsic neurite growth programs to amacrine cells' varied neurite morphologies in vivo.

Methods

Amacrine Cell and RGC Purification

Sprague-Dawley rats were used for these experiments in compliance with institutional animal care and use committee review and approval. All animals were treated in accordance with the ARVO Statement for the Use of Animals in Ophthalmic and Vision Research. Amacrine cells and RGS were purified by immunopanning as previously described.[8–11] Briefly, retinas were dissected from embryonic day 20 (E20) and postnatal days 8 through 10 (P8–P10) rats and dissociated with papain (Worthington, Lakewood, NJ) using gentle mechanical trituration to obtain a single-cell suspension. After depleting the retinal suspension of macrophages, RGCs were positively selected using T11d7 monoclonal antibodies.[12] Enrichment of

Copyright 2013 The Association for Research in Vision and Ophthalmology, Inc.

Downloaded from iovs.arvojournals.org on 04/15/2021

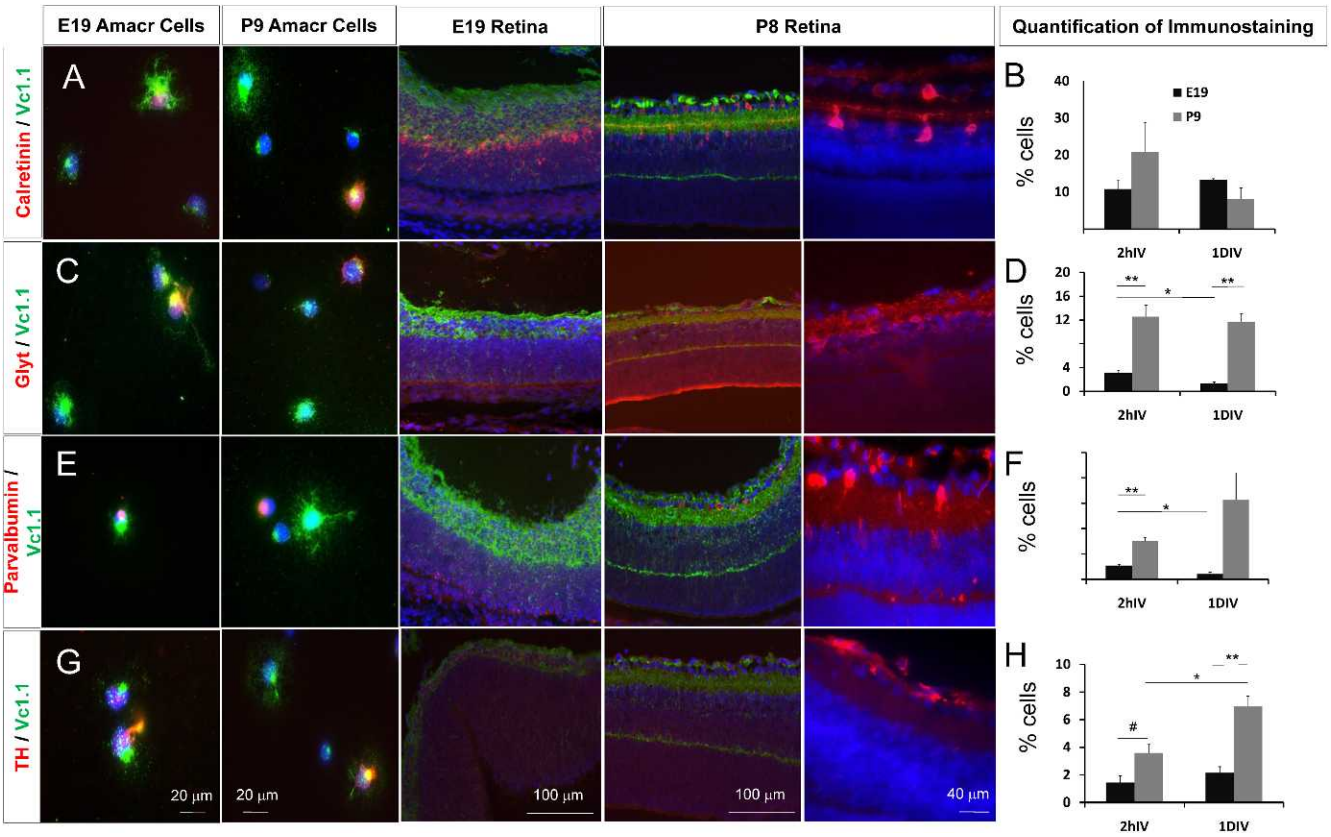

Figure 1. Immunostaining of amacrine cells in vitro and in vivo. **(A, C, E, G)** E19 or P8 amacrine cells were purified, plated in serum-free media and immunostained as labeled. E19 and P8 retinal cross-sections were stained for the same amacrine cell markers. **(B, D, F, H)** Quantification of immunoreactivity of amacrine cells in vitro at 2 hours in vitro or 1DIV after plating for each marker as labeled. #$P = 0.055$ "trend." *$P < 0.05$; **$P < 0.01$; Student's *t*-test.

amacrine cells to ~90% purity was achieved subsequently by depleting Ox7-positive cells (remaining RGCs and other retinal neurons), and immunopanning for Vc1.1-positive cells.[13]

Amacrine Cell and RGC Culture

Acutely purified amacrine cells and RGCs were plated at low density on poly-d-lysine (PDL)-coated glass coverslips (70 kDa, 10 µg/mL; Sigma-Aldrich, St. Louis, MO), without and with laminin, respectively (Trevigen, Gaithersburg, MD) in serum-free media (Neurobasal; Gibco, Carlsbad, CA) as described[8,9,11] containing insulin (50 ng/mL) and forskolin (5 mM; Sigma-Aldrich); ciliary neurotrophic factor (10 ng/mL; Peprotech, Rocky Hill, NJ), brain-derived neurotrophic factor (50 ng/mL; Peprotech), and a modified version of B27.[14] Under these conditions, survival of amacrine cells at 3 days in vitro (3DIV) is ~60%.[11] Cultures were maintained at 37°C in a humidified incubator with 10% CO_2 and either immunostained or processed for neurite growth analysis as described below.

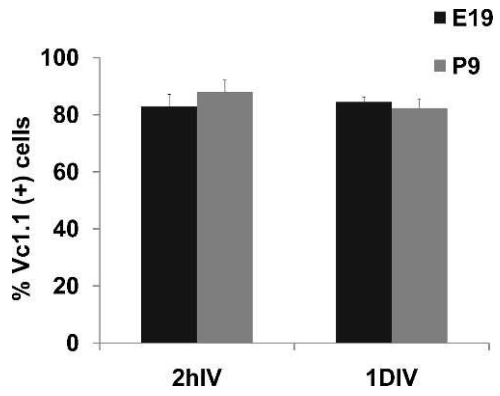

Figure 2. Amacrine cell immunostaining with Vc1.1 antibody. Acutely purified amacrine cells were plated in serum-free media and immunostained at 2 hours or at 1DIV. The *bars* show percentage of cells immunopositive for Vc1.1 of the total number of cells labeled with the nuclear dye DAPI. *Error bars*: SEM.

Immunofluorescence

For immunostaining of the retina, eyes were dissected from E20 and P9 Sprague-Dawley rats. Corneas and vitreous bodies were carefully removed and the eyecups were immediately fixed with 4% paraformaldehyde for 2 hours, after which the tissues were cryoprotected in 30% sucrose, snap frozen in mounting medium (OCT Tissue-Tek; Electron Microscopy Sciences, Hatfield, PA), and sectioned. Sections were postfixed in 4% paraformaldehyde or 10% trichloroacetic acid (TCA) for 10 minutes, then blocked and permeabilized with 20% goat or donkey serum and 0.2% Triton X-100 for 30 minutes. Retinal tissues were incubated overnight with anti-Vc1.1 (1:100; Sigma-Aldrich), anti-HPC-1 (1:200; Abcam, Cambridge, MA), anti-parvalbumin (PV, 1:500; Sigma-Aldrich), anti-calretinin (1:5000), anti-glutamate transporter 1 (GLYT-1, 1:2000) and anti-tyrosine hydroxylase (TH, 1:100; BD Biosciences, Mississauga, ON, Canada). Secondary detection was performed using fluorescent antibodies at a 1:500 (Alexa-488, Alexa-594) or a 1:200 dilution (Alexa-647; Invitrogen, Carlsbad, CA). The slides

Investigative Ophthalmology & Visual Science

Downloaded from iovs.arvojournals.org on 04/15/2021

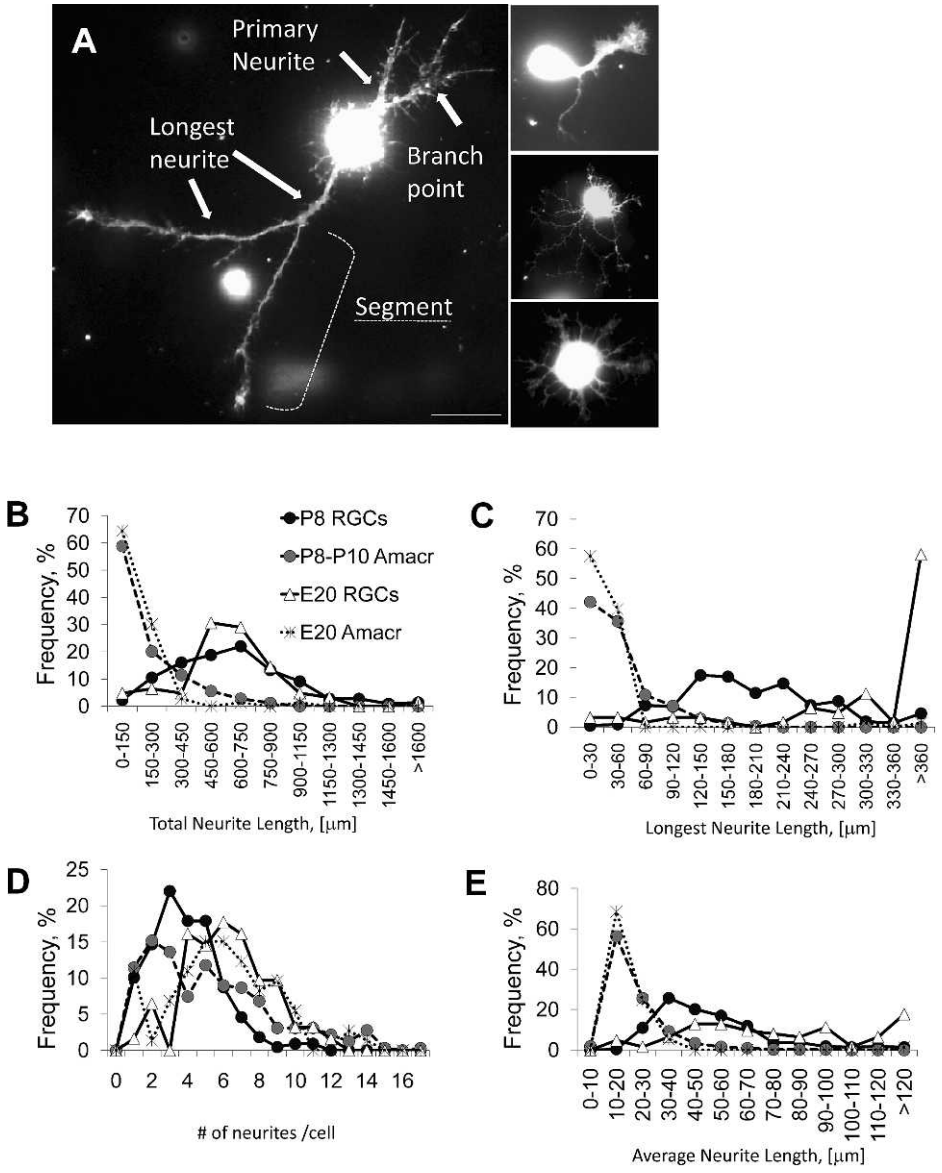

Figure 3. Different populations of amacrine cells can be identified by their polarization patterns in vitro. (**A**) Postnatal day 9 amacrine cells were purified by immunopanning and cultured in the presence of trophic factors. After 3 days in vitro, the cells were fixed and stained with TRITC-conjugated phalloidin. Images were analyzed in a fluorescence microscope and the neurites were manually traced using microscopy software. *Scale bar*: 20 μm. (**B–E**) Postnatal amacrine cells and RGCs were purified and plated for 3 days, after which cells were stained with phalloidin and their neurites manually traced (E20 RGCs, $n = 62$; E20 amacrines, $n = 73$; postnatal RGCs, $n = 218$; postnatal amacrine cells, $n = 323$).

were mounted in medium with DAPI (Vectashield; Vector Laboratories, Burlingame, CA) and examined with an inverted fluorescent microscope (Axio Observer Z1; Carl Zeiss Microscopy, Thornwood, NY) or a confocal microscope (Leica TCS SP5; Leica Microsystems, Buffalo Grove, IL).

Immunocytochemistry of purified amacrine cells as in Figure 1 was performed at 2 and at 24 hours after plating the cells on PDL-coated glass coverslips (70 kDa, 10 μg/mL; Sigma-Aldrich) in serum-free media. Antibodies used are described above.

Phalloidin Staining and Neurite Growth Analysis

Amacrine cells and retinal ganglion cells were acutely purified from embryonic (E20) and postnatal (P8–P11) animals and plated at clonal density on glass coverslips (70 kDa, 10 μg/mL; Sigma-Aldrich) in serum-free media as described above. After 3DIV, cells were carefully fixed with warm 4% paraformaldehyde for 25 minutes. Blocking and membrane permeabilization were performed as described above and TRITC-conjugated phalloidin (3.3 g/mL; Sigma-Aldrich) was added and left overnight at 4°C together with DAPI (Invitrogen) for nuclear staining. Neurite length measurements were performed at ×20 and ×63 objective magnification using an inverted fluorescence microscope and microscopy software (AxioVision; Carl Zeiss Microscopy); data analysis was conducted using spreadsheet software (Excel; Microsoft Corp., Redmond, WA) and statistical software (SPSS; IBM, Chicago, IL). At least 60 cells were analyzed per experiment. Five different variables were recorded for each cell: number of primary neurites coming off the cell body $\geq$ 10 μm and their individual length, number of branch points with branches $\geq$ 10 μm and the neurite length of each branch, and length of the longest neurite without its branches. Combination of these values allowed for the

Investigative Ophthalmology & Visual Science

Downloaded from iovs.arvojournals.org on 04/15/2021

Table 1. Comparison of Neurite Growth Variables in Amacrine Cells and RGCs

	Amacrines P8–P10	Amacrines E20	RGCs P8	RGCs E20	Total	ANOVA, K-W *P* Value	Post Hoc Comparison Results
Number of segments							
Mean	8.76	7.67	14.27	8.55	10.40	<0.001, <0.001	RGCs P8 > Amacrines P8–P10,
SD	7.73	5.61	8.71	3.87	8.05		Amacrines E20, RGCs E20
Median	7.00	7.00	12.00	8.00	8.00		
Minimum	1.00	1.00	1.00	1.00	1.00		
Maximum	50.00	36.00	57.00	17.00	57.00		
Number of neurites > 10 μm							
Mean	5.24	5.92	3.89	6.23	4.97	<0.001, <0.001	RGCs E20, Amacrines E20 >
SD	3.48	2.95	1.96	2.36	3.02		RGCs P8 Amacrines E20 >
Median	5.00	6.00	4.00	6.00	5.00		RGCs P8 Amacrines P8–P10 >
Minimum	1.00	1.00	1.00	1.00	1.00		RGCs P8
Maximum	17.00	14.00	11.00	12.00	17.00		
Number of branch points with branches > 10 μm							
Mean	1.76	0.88	5.19	1.16	2.71	<0.001, <0.001	RGCs P8 > Amacrines P8–P10,
SD	2.70	1.95	4.13	1.40	3.54		Amacrines E20, RGCs E20
Median	1.00	0.00	5.00	1.00	1.00		Amacrines P8–P10 > Amacrines
Minimum	0.00	0.00	0.00	0.00	0.00		E20
Maximum	18.00	13.00	26.00	5.00	26.00		
Branching index							
Mean	0.34	0.12	1.77	0.20	0.76	<0.001, <0.001	RGCs P8 > Amacrines P8–P10,
SD	0.52	0.22	1.91	0.32	1.34		Amacrines E20, RGCs E20
Median	0.11	0.00	1.25	0.12	0.29		Amacrines P8–P10, RGCs E20 >
Minimum	0.00	0.00	0.00	0.00	0.00		Amacrines E20
Maximum	3.00	1.30	16.00	2.00	16.00		
Average segment length							
Mean	21.84	21.38	51.27	101.55	38.59	<0.001, <0.001	RGCs E20 > RGCs P8 >
SD	11.81	24.71	24.37	105.40	43.69		Amacrines P8–P10, Amacrines
Median	18.42	16.97	45.58	76.61	27.12		E20
Minimum	7.34	10.85	18.29	13.39	7.34		
Maximum	92.27	223.82	202.06	682.67	682.67		
Average neurite length							
Mean	34.35	25.28	204.37	125.37	96.55	<0.001, <0.001	RGCs P8 > RGCs E20 >
SD	23.59	25.20	144.96	103.14	119.50		Amacrines P8–P10 > Amacrines
Median	28.07	21.04	178.04	99.38	46.38		E20
Minimum	10.35	10.93	18.29	13.39	10.35		
Maximum	170.11	223.82	1098.76	682.67	1098.76		
Longest neurite length							
Mean	45.22	47.20	195.05	430.29	129.07	<0.001, <0.001	RGCs E20 > RGCs P8 >
SD	32.81	126.48	88.21	272.38	158.92		Amacrines P8–P10, Amacrines
Median	33.37	27.05	180.04	387.99	63.56		E20
Minimum	10.35	10.93	20.28	19.98	10.35		
Maximum	180.07	1068.49	689.24	1727.41	1727.41		
Total neurite length							
Mean	184.35	151.38	643.16	642.90	370.80	<0.001, <0.001	RGCs P8, RGCs E20 > Amacrines
SD	173.26	151.11	323.97	287.36	332.51		P8–P10, Amacrines E20
Median	121.77	123.35	615.19	631.18	266.31		
Minimum	10.35	10.93	18.29	78.00	10.35		
Maximum	861.32	1119.10	2073.63	1778.81	2073.63		

Since variances are significantly different between cell types for all variables, ANOVA overall group comparison were verified with the Kruskal-Wallis test, followed by Tamhane's multiple comparison procedure.

calculation of the rest of the parameters used in data analysis: total neurite length (sum of the length of all primary neurites and their branches); number of segments (number of primary neurites + 2 × number of branch points); and average segment length (total neurite length divided by the number of segments). Comparison of neurite growth variables by cell type yielded significantly high variances between cell types for all variables; therefore, ANOVA overall group comparison were verified with the Kruskal-Wallis test, followed by Tamhane's multiple comparison procedure.

Investigative Ophthalmology & Visual Science

Downloaded from iovs.arvojournals.org on 04/15/2021

Table 2. Principal Component Analysis

	P8–P10 Amacrines			E20 Amacrines			P8 RGCs			E20 RGCs		
Principal Component Analysis	**PC1**	**PC2**	**PC3**	**PC1**	**PC2**	**PC3**	**PC1**	**PC2**	**PC3**	**PC1**	**PC2**	**PC3**
Number of segments	**0.21**	*−0.23*	*−0.13*	**0.15**	*−0.26*	*−0.16*	**0.26**	*−0.22*	0.04	**0.25**	*−0.22*	*−0.14*
Number of neurites > 10 μm	**0.16**	*−0.12*	*−0.47*	**0.10**	*−0.17*	*−0.81*	0.00	*−0.44*	*−0.16*	0.03	*−0.17*	*−0.49*
Number of branch points > 10 μm	**0.19**	*−0.24*	**0.12**	**0.14**	*−0.25*	**0.38**	**0.27**	*−0.13*	0.08	**0.32**	*−0.15*	**0.23**
Branching index	**0.13**	*−0.16*	**0.53**	**0.13**	*−0.25*	**0.44**	**0.23**	**0.25**	**0.16**	**0.27**	*−0.11*	**0.41**
Average segment length	0.08	**0.48**	−0.06	**0.18**	**0.23**	0.02	−0.09	**0.15**	*−0.45*	0.07	**0.26**	0.03
Average neurite length	**0.17**	**0.22**	**0.38**	**0.22**	**0.16**	**0.13**	**0.20**	**0.35**	−0.02	**0.17**	**0.24**	**0.15**
Longest neurite length	**0.17**	**0.31**	−0.06	**0.21**	**0.19**	0.04	0.08	**0.12**	*−0.45*	**0.24**	**0.19**	*−0.23*
Total neurite length	**0.22**	0.04	*−0.18*	**0.24**	0.04	*−0.18*	**0.22**	*−0.14*	*−0.30*	**0.32**	**0.10**	*−0.35*
Variance explained, %	53	24	18	50	37	12	42	25	23	29	44	19

Negative component coefficients (*italic*) for a variable indicate that cells with large values for that observed variable tend to sort toward one end of that underlying variable, while positive coefficients (*bold*) indicate they sort toward the other end of that underlying variable. Coefficients with absolute value < 0.1 indicate that the observed variable does not contribute much to the underlying principal component.

Neurite Growth Analysis of Amacrine Cell Subpopulations

Postnatal day 8 amacrine cells were purified and plated on PDL-coated coverslips as described above. At 3DIV, cells were carefully fixed in warm 4% PFA and processed for immunostaining and phalloidin labeling as previously described. Cells were manually traced as indicated in the phalloidin (neurites) channel to mask the observer, and grouping of cells by immunoreactivity to amacrine cell subtype markers was assessed later on. Measurements of immunoreactive cells were compared against their negative counterparts within the same group. At least 50 immunoreactive cells were analyzed per group and the means were compared using unpaired Student's *t*-test.

Results

Purified Amacrine Cell Subpopulations During Development

We purified E20 and P9 amacrine cells by immunopanning and asked whether these amacrine cell subpopulations change greatly through the early embryonic to late postnatal period. We immunostained acutely purified cells at either 2 hours after

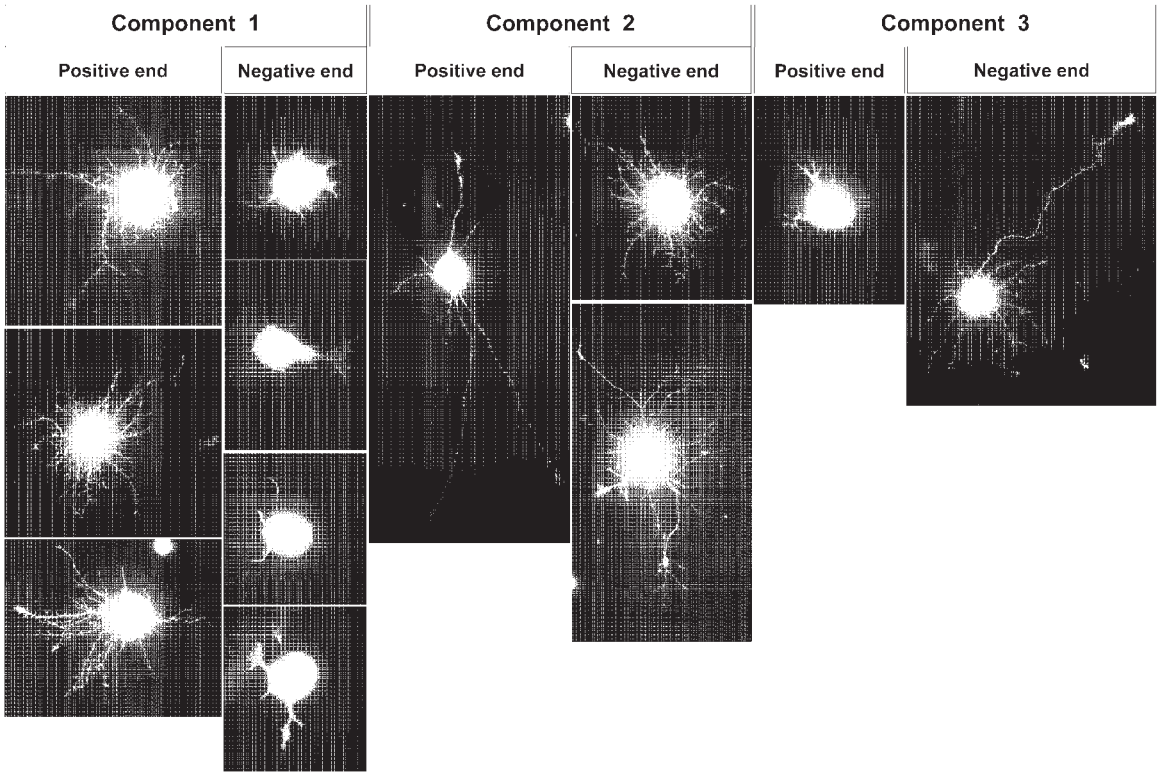

Figure 4. Amacrine cell morphology in vitro and contribution to principal component analysis. Example images of postnatal amacrine cells at the extremes of the principal component axes described in Table 2 are shown here. Scale varies slightly to demonstrate neurite growth in each picture.

Investigative Ophthalmology & Visual Science

Downloaded from iovs.arvojournals.org on 04/15/2021

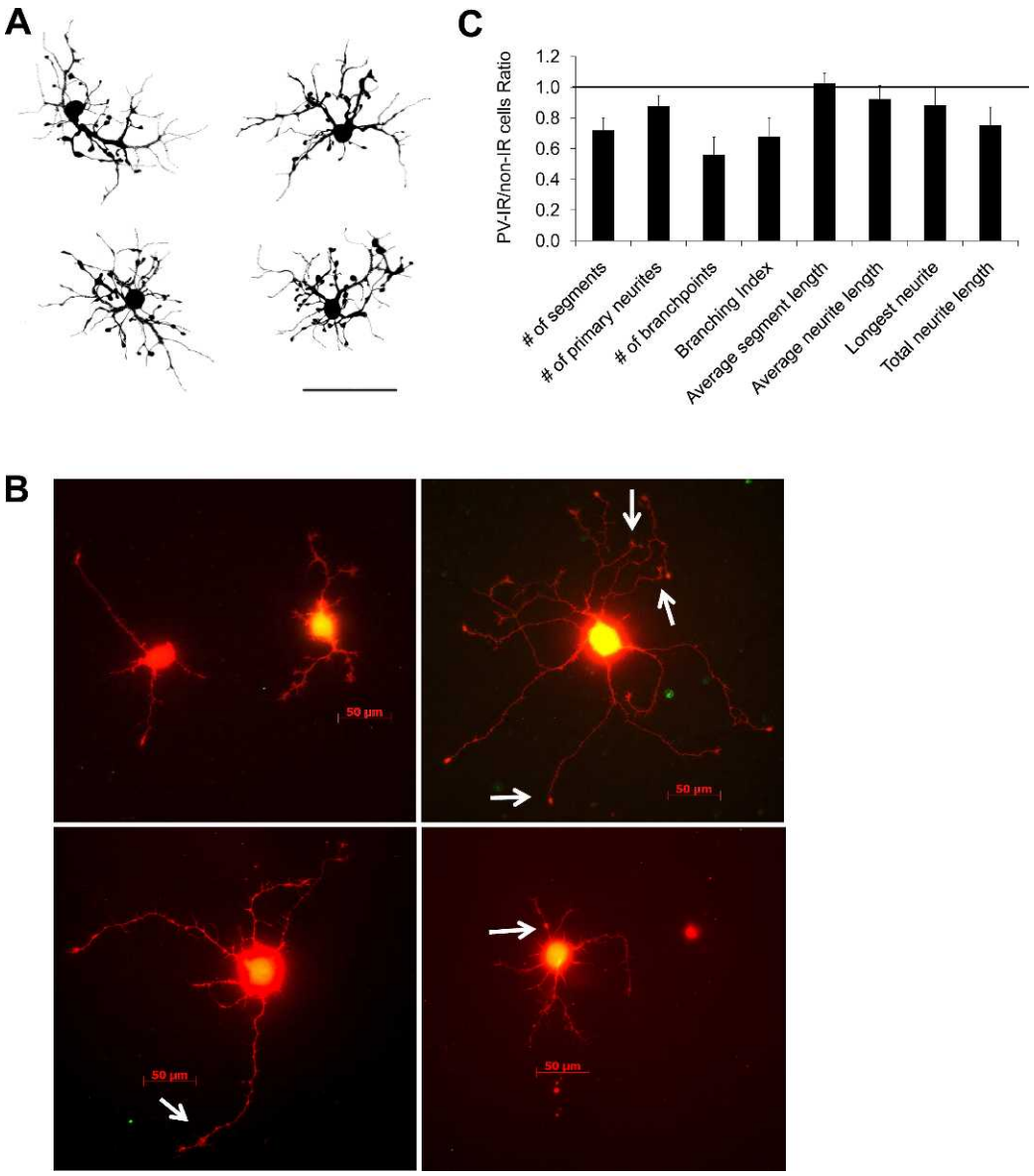

Figure 5. Parvalbumin immunoreactive amacrine cells in vivo and in vitro. (**A**) Camera lucida reconstructions of parvalbumin immunoreactive cells from rabbit inferior retina. Reprinted with permission from Casini G, Rickman DW, Brecha NC. AII amacrine cell population in the rabbit retina: identification by parvalbumin immunoreactivity. *J Comp Neurol*. 1995;356:132–142. Copyright 1995 Wiley-Liss, Inc. (**B**) Purified amacrine cells immunoreactive to parvalbumin (*yellow*) and counterstained with TRITC-conjugated phalloidin show a similar morphology in vitro. The *arrows* show examples of lobular processes. (**C**) Quantification of neurite growth parameters of PV-IR amacrine cells at 3DIV. The *bars* represent the values of PV-IR cells ($n = 70$ cells) normalized to non-IR cells within the experiment ($n = 53$ cells). *Error bars*: SEM of the PV-IR cells.

plating or at 1DIV, and found that, at 2 hours in vitro, fewer E19 amacrine cells were immunoreactive to GLYT-1 (Figs. 1C, 1D), PV (Figs. 1E, 1F), and TH (trend level only; Figs. 1G, 1H) than P9 amacrine cells, whereas calretinin immunoreactivity was statistically similar at the two ages (Figs. 1A, 1B). After 1 DIV, E19 amacrine cells conserved their immunoreactivity to TH and Vc1.1 (Fig. 1H, Fig. 2), but decreased in immunoreactivity to GLYT-1 and PV (Figs. 1D, 1F), due to either in vitro aging or a relative decrease in survival of these cells at this particular developmental age. We found no significant changes in immunoreactivity of P9 amacrine cells from 2 hours to 1DIV (Figs. 1B, 1D, 1F), except for an increase in TH-immunoreactive (TH-IR) cells (Fig. 1H). Immunostaining of retinal cross-sections showed similar differences in amacrine cell subpopulation immunoreactivity for calretinin, GLYT-1, PV, and TH between E19 and P8 (Fig. 1). Taken together, these data suggest that significant amacrine cell differentiation, at least in the expression of this subset of subpopulation markers, continues through this developmental period, consistent with prior literature on the coordinated expression of neurotransmitters at all stages during retinal development.[15–19] Importantly, we found that these subtype marker phenotypes are expressed in mostly stable proportions in vitro.

Amacrine Cell Neurite Extension In Vitro

Amacrine cells extend complex and varied neurites in vivo; the variation in their neurite patterning has been used to characterize them in vivo into subtypes based on morphology.[3,7,20] We asked whether this varied morphology is recapitulated in vitro. We purified embryonic and postnatal amacrine cells and cultured them in defined, serum-free media. At 3DIV,

Investigative Ophthalmology & Visual Science

Downloaded from iovs.arvojournals.org on 04/15/2021

Table 3. Neurite Growth Statistics of PV-IR Cells

Variable	Group	*n*	Mean	SD	SEM	*t*-test for Equality of the Means – Significance, 2-tailed; equal variance not assumed
Number of segments	IR cells	70	6.4571	6.18949	0.73979	0.106
	Non-IR cells	53	8.9811	9.86347	1.35485	
Number of primary neurites	IR cells	70	3.9714	2.55361	0.30521	0.297
	Non-IR cells	53	4.5283	3.15987	0.43404	
Number of branch points	IR cells	70	1.2429	2.18317	0.26094	0.105
	Non-IR cells	53	2.2264	3.93036	0.53988	
Branching index	IR cells	70	0.3037	0.45238	0.05407	0.146
	Non-IR cells	53	0.4468	0.5924	0.08137	
Average segment length	IR cells	70	24.1314	12.87655	1.53904	0.794
	Non-IR cells	53	23.5734	10.78301	1.48116	
Average neurite length	IR cells	70	39.1857	31.18085	3.72682	0.576
	Non-IR cells	53	42.4491	32.56867	4.47365	
Longest neurite	IR cells	70	48.1316	53.70092	6.41849	0.533
	Non-IR cells	53	54.6443	59.60329	8.18714	
Total neurite length	IR cells	70	160.9063	212.31594	25.37661	0.266
	Non-IR cells	53	214.1643	292.91882	40.23549	

amacrine cells were stained with phalloidin to visualize neurite morphology and their neurites were manually traced (Fig. 3A). We collected data on five different parameters of neurite growth: the number of primary neurites extending from the cell body, the number of branch points, the length of each primary neurite with its branches, the length of every branch, and the length of the longest neurite without its branches. We used these data to calculate three additional variables: the total neurite length; the number of segments (defined as a stretch of neurite bounded by the cell body, a branch point, or the end of a neurite); and the average segment length (see Methods and Fig. 3A).

We analyzed these different neurite growth parameters and found that postnatal amacrine cells were able to extend multiple neuritis; and in some cases, one of the neurites was as long as 180 μm (longest neurite; see Table 1), although the majority of the cells (60%) extended neurites less than 150 μm long (Fig. 3B). Consistent with the existence of axon-bearing amacrine cells,[21,22] in our cultures we found that ~40% of the postnatal amacrine cells extended one lengthy process, typically 20 to 40 μm long (Fig. 3C).

Embryonic amacrine cells also grew one lengthier neurite of similar size on average (47 μm). Comparing this phenomenon with RGCs, we found that postnatal RGCs, on average, have a longest neurite (axon) 4 times larger (195 μm) and that in embryonic RGCs, the longest neurite is almost 10 times as long (430 μm; Table 1). Thus embryonic and postnatal amacrine cells extend neurites of similar lengths, unlike RGCs, which extend considerably longer axons in the embryonic period than in the postnatal period.[8]

Quantifying the number of neurites per cell and the average segment length roughly grouped the amacrine cells into clusters (Figs. 3D, 3E) suggesting the existence of more than one cell subpopulation in our cultures. To address this observation, and ask whether in vitro amacrine cells retain morphologic diversity analogous to that exhibited in vivo, we performed a principal component analysis. This is a multivariate analysis method that reduces our original seven variables into fewer components when (and if) these variables are highly correlated. We found that three components were able to explain 90% to 99% of the variance in the samples analyzed (Table 2). Component 1, which accounted for approximately 53% of the variability in amacrine cell neurite growth, described a variable largely based on total neurite growth capacity, with a spectrum running from short, simple cells on one end to long, complex neurite morphologies on the other (example cells in Fig. 4). Component 2, which explained 24% of the variability in amacrine cell neurite growth, ran from short, highly branched neurites on one end to long neurites with fewer branches on the other (Fig. 4). This suggests that a significant component of neurite growth can be explained by a mechanism that trades branching for total length. Finally, component 3 accounted for 18% of the variability, and displayed a wide spectrum of neurite shape and length complexity, where large numbers of neurites and longer lengths were on one end and large numbers of branches were on the other end (Fig. 4). Interestingly, the principal component analysis yielded remarkably similar data for embryonic and postnatal amacrine cells and postnatal RGCs (Table 2), but embryonic RGCs differed slightly in that they had the longest neurite length per neuron and a corresponding larger average segment length (Table 1), and their "component 2," trading length for branching, was extracted first and explained the most variance (29%) rather than the second most, as in all of the other populations studied (Table 2). Thus, these data suggest that "component 2" (trading branching versus length) is more important for characterizing E20 RGCs than "component 1" (overall size), whereas for postnatal RGCs and amacrine cells at all ages, overall size is a more important feature of neurite growth.

Neurite Outgrowth of Amacrine Cell Subpopulations

Extensive evidence suggests that extrinsic, environmental signals are critical for shaping amacrine cell morphologies in vivo, but there is less evidence that addresses whether the variety of morphologies in vivo also depends on an intrinsic or cell-autonomous component (see Discussion below). To address this question, we asked whether purified amacrine cells would retain any intrinsic neurite growth properties typical of their in vivo growth patterns. We purified amacrine cells, characterized them by immunocytochemistry and measured their neurite outgrowth as described in the Methods section.

Investigative Ophthalmology & Visual Science

Downloaded from iovs.arvojournals.org on 04/15/2021

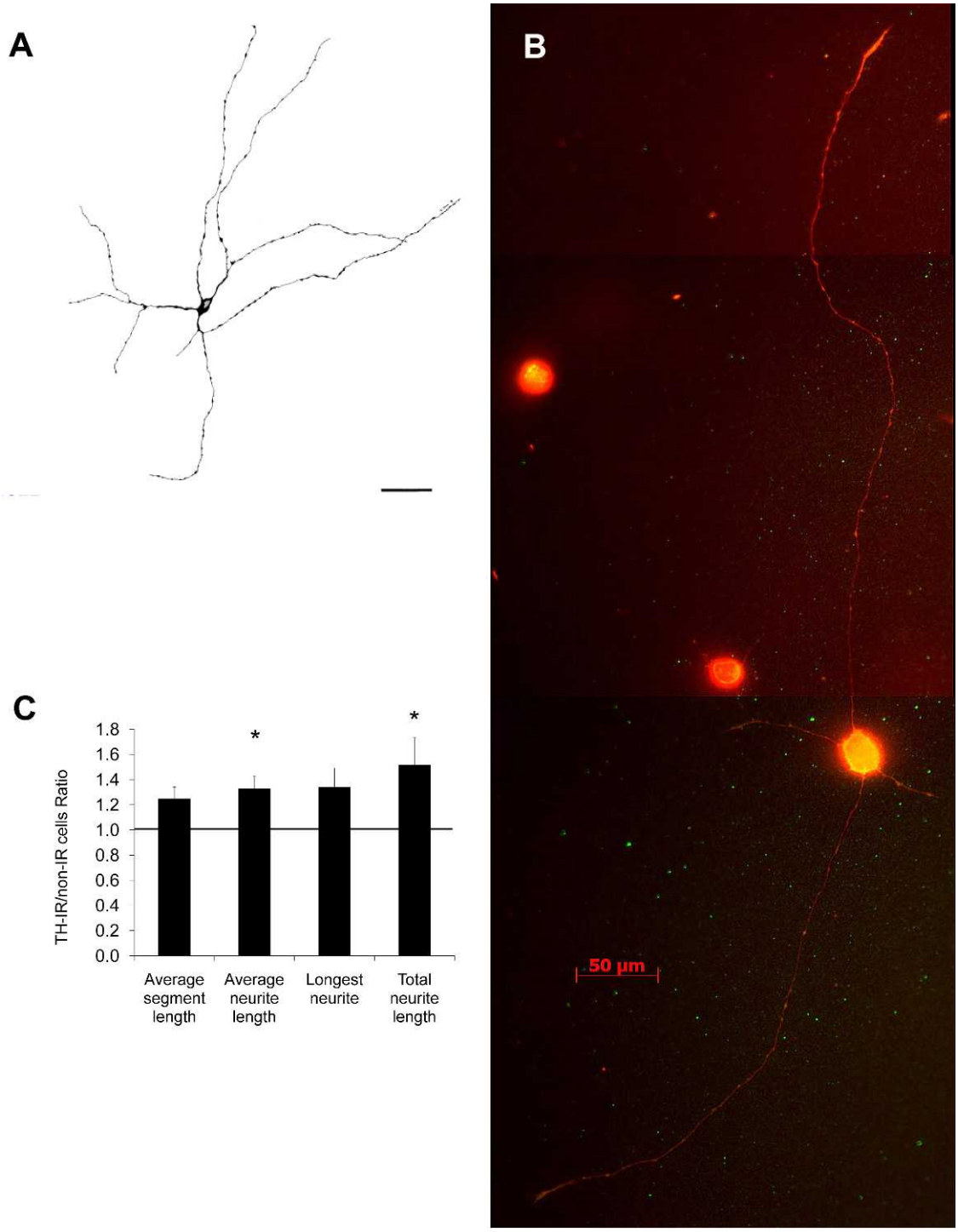

Figure 6. Tyrosine hydroxylase immunoreactive amacrine cells in vivo and in vitro. (**A**) Camera lucida reconstructions of tyrosine hydroxylase immunoreactive cells in the ventral part of adult rabbit retina. Reprinted with permission from Casini G, Brecha NC. Postnatal development of tyrosine hydroxylase immunoreactive amacrine cells in the rabbit retina: I. Morphological characterization. *J Comp Neurol*. 1992;326:283–301. Copyright 1992 Wiley-Liss, Inc. *Scale bar*: 50 µm. (**B**) Purified amacrine cells immunoreactive to tyrosine hydroxylase (*yellow*) and counterstained with TRITC-conjugated phalloidin show a similar morphology in vitro. (**C**) Quantification of neurite growth parameters of TH-IR amacrine cells at 3DIV. The *bars* represent the values of TH-IR cells ($n = 88$ cells) normalized to non-IR cells within the experiment ($n = 56$ cells). $^*P < 0.05$, unpaired Student's *t*-test. *Error bars*: SEM of the TH-IR cells.

We first asked whether parvalbumin-immunoreactive (PV-IR) amacrine cells in vitro would replicate their in vivo morphologies. Previous camera lucida reconstructions of PV-IR cells of the rabbit retina show cells with a pyriform cell body and cell processes with lobular appendages in one sublamina and arboreal processes in another sublamina[23] (Fig. 5A), consistent with the description of AII amacrine cells revealed by the use of intracellular labels such as Golgi stain,[24] horseradish peroxidase, and Lucifer Yellow.[25] We found that PV-IR cells trended toward lower number of segments, number

Investigative Ophthalmology & Visual Science

Downloaded from iovs.arvojournals.org on 04/15/2021

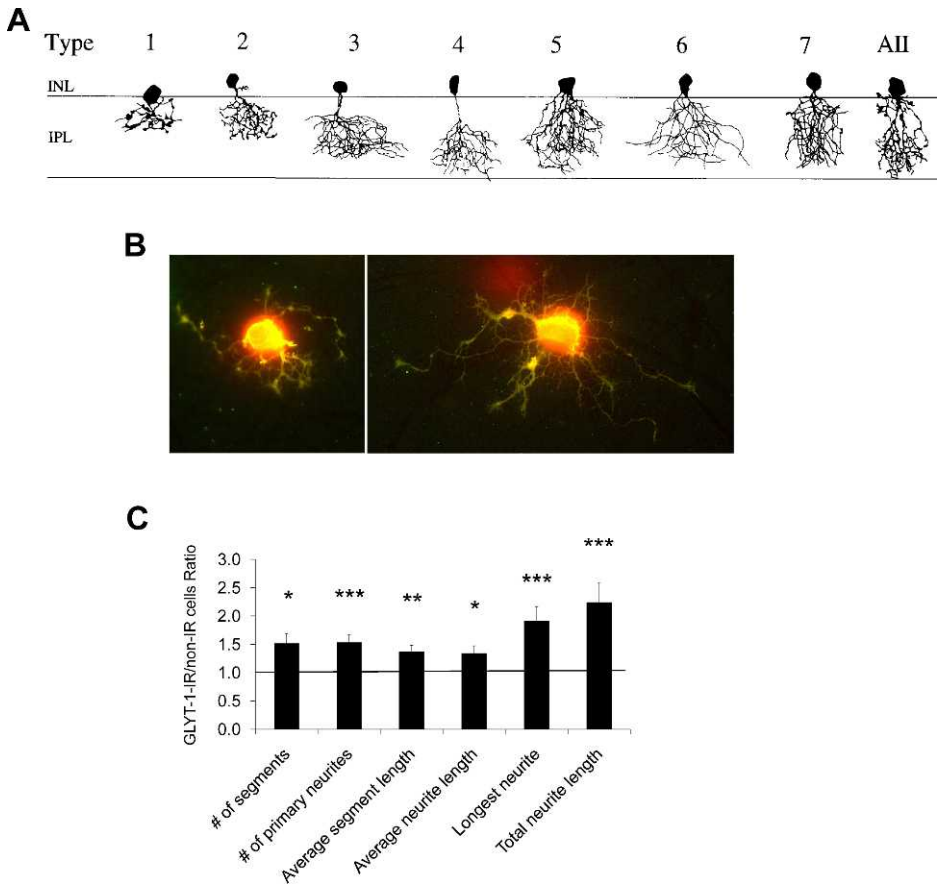

FIGURE 7. GLYT-1 immunoreactive amacrine cells in vivo and in vitro. (**A**) Illustrations of eight types of GLYT-IR cells from rat retina spanning different sublaminae of the IPL. Reprinted with permission from Menger N, Pow DV, Wässle H. Glycinergic amacrine cells of the rat retina. *J Comp Neurol*. 1998;401:34–46. Copyright 1998 Wiley-Liss, Inc. (**B**) Purified amacrine cells immunoreactive to GLYT-1 (*yellow*) and counterstained with TRITC-conjugated phalloidin show a similar morphology in vitro. (**C**) Quantification of neurite growth parameters of GLYT-1-IR amacrine cells at 3DIV. The *bars* represent the values of GLYT-1-IR cells ($n = 67$ cells) normalized to non-IR cells within the experiment ($n = 67$ cells). $^{*}P < 0.05$. $^{**}P < 0.01$. $^{***}P < 0.001$, unpaired Student's *t*-test. *Error bars*: SEM of the GLYT-1-IR cells.

of primary neurites coming off the cell body, number of branch points, longest neurite, and total neurite length compared with non–PV-IR amacrine cells (Figs. 5B, 5C). However, because of the high variability of these values (Table 3), the difference between the means was not statistically significant. PV-IR cells did demonstrate lobular varicosities on their neurites in vitro similar to those seen in vivo (arrows in Fig. 5B). Thus PV-IR amacrine cells in vitro demonstrate a morphology similar to that in vivo (Fig. 5B).

We next investigated the morphology of TH-IR cells in vitro. These cells are part of the family of wide field amacrine cells and in vivo, they have been described as cells with long (hundreds of micrometers), thin, unbranched, axon-like processes with few spines or varicosities[3,22,26–28] (Fig. 6A). Consistent with their morphology in vivo, TH-IR amacrine cells in vitro extended fewer primary neurites that were 33% longer on average than those of non–TH-IR amacrine cells. Overall, the total neurite length of TH-IR cells was 50% larger than in non–TH-IR amacrine cells (Figs. 6B, 6C). Thus, for TH-IR cells, there was striking morphological similarity among purified amacrine cells and the cells described in the literature in the mammalian retina (Fig. 6A).[3,26,27]

Finally, we examined the morphology of glycinergic amacrine cells in vitro and found that they too resembled the shape of glycinergic amacrine cells in vivo (Figs. 7A, 7B).[29] Glycinergic amacrine cells, widely known as AII amacrine cells, are characterized by their narrow field and a bushy dendritic tree coming off a single neurite that can span many sublaminae in the inner plexiform layer (IPL; Fig. 7A). In our cultures, cells that were immunoreactive to the glycinergic transporter 1 (GLYT-1-IR cells) had a significantly greater number of segments and a total neurite length ~2-fold larger than controls (Fig. 7C). The number of primary neurites coming off the cell body was significantly higher in GLYT-1-IR cells (Figs. 7B, 7C). Taken together, these data show that in vitro, amacrine cells elaborate neurites with a variety of complexities reminiscent of the variation in patterning seen in vivo, and support the hypothesis that at least a portion of their patterning variability in vivo may depend on cell-intrinsic mechanisms.

DISCUSSION

Understanding the molecular and cellular basis for the morphological heterogeneity of neurons in the central nervous system remains a major goal in neuroscience. Amacrine cells in the mammalian retina represent an excellent model system in which to study this question, as they demonstrate remarkable morphologic heterogeneity[1,2,30,31]—despite arising from a common progenitor,[32–38] migrating to only two retinal layers, and extending neurites into the same synaptic neuropil, the inner plexiform layer of the retina. Although the variation in amacrine cell morphology has been carefully characterized in

Investigative Ophthalmology & Visual Science

Downloaded from iovs.arvojournals.org on 04/15/2021

vivo, little work has focused on which of their properties are maintained cell autonomously in vitro. Similar work on other populations of central nervous system neurons has yielded fruitful observations about neurite growth properties; for example, the signals optimal for survival and neurite growth of RGCs have been characterized using such cultures.[39,40] Here we take advantage of our ability to highly purify these neurons by immunopanning to study their neurite growth away from neuronal- or glial-derived signals found in the in vivo environment.

Total Neurite Length Conservation in Amacrine Cell Neurite Growth

Detailed analysis of neurite morphology in vivo has suggested that at least some neurons maintain a constant total neurite length when they grow neurites, trading off between neurite length and branching.[41] Our data using principal component analysis suggest that the second greatest component that captures the variance in amacrine cell neurite growth follows this principle of trading neurite length for complexity (branching), and supports the hypothesis that the biology that underlies this observed conservation may be cell-autonomous. The increased importance of this conservation principle in embryonic RGCs (Table 2) may ultimately explain their dramatically increased axon growth ability compared with either amacrine cells, or with postnatal or adult RGCs.[8] The underlying biology could in theory involve limitations on supply of any single or number of building blocks for neurite elongation (e.g., cytoplasmic or membrane components[42]) or we hypothesize a feedback between the cell body and neurites or growth cones, but remains to be discovered.

Intrinsic Regulation of Amacrine Cell Neurite Growth

It is not known whether the varied morphology of amacrine cell neurites in vivo[1–3] is attributable to cell intrinsic or extrinsic signals, or both. Evidence for the role of extrinsic cues in neurite patterning in the retina came from experiments addressing the role of activity in RGCs' dendrite remodeling during development. In these experiments, a decrease in local calcium concentration at the tip of the dendrites was sufficient to alter the dendritic organization of RGCs.[6] Further evidence for the importance of extrinsic cues in neurite patterning was demonstrated in mutant zebrafish, where in the absence of RGCs, amacrine cells failed to properly direct their projections to the IPL and the sublaminar architecture of the retina was temporarily disorganized.[5] Over time, most of the projection errors were corrected and the sublaminae were formed, suggesting that the IPL contained other cues, including possibly the amacrine cell neurites themselves that were important for lamination.[4]

Here we find that a number of amacrine cell subtypes recapitulate aspects of their in vivo morphology in vitro. Consistent with prior characterizations of amacrine cell subpopulations in the mammalian retina,[2,26,29,43–47] in our cultures PV-IR cells grew processes with lobular appendages and multiple varicosities.[23,48] TH-IR cells had long axon-like, unbranched processes,[22] and GLYT-1-IR cells also exhibited a typical bushy neurite morphology,[29] although our quantitative analysis of number of branch points and branching index of GLYT-1-IR cells did not yield statistically significant differences with the non-IR cells, possibly because our analyses did not include branches < 10 μm. Nevertheless, these data suggest that amacrine cells have cell subtype-specific intrinsic determinants of neurite growth that are carried into culture.

Despite the strong evidence for the role of extrinsic cues in determining neurite patterning in the developing retina, a few prior results support the hypothesis of intrinsic regulation. For example, during the initial phase of lamination in the developing zebrafish retina, amacrine cells extend processes indiscriminately that are not directed toward their final destination, the IPL.[4] This may represent a brief developmental period of neurite growth relatively free of guidance from extrinsic cues. The culture model used here may be useful to study such guidance cues in the future, although there are certain limitations to studying amacrine cell neurite growth in vitro, such as the lack of three-dimensional (3-D) cues to study neurite polarity, or to investigate neurite lamination into separate layers, as occurs in the IPL.

The creation of transgenic mouse lines that express fluorescent protein reporters under the control of amacrine cell-specific promoters (for example, as in Haverkamp et al.[50]) and the existence of eletrospun scaffolds to study RGC properties in 3-D[49] and scaffolds that support RGC and amacrine cell survival[51] will certainly allow these questions to be further addressed. Taken together, these data support the existence of genetically programmed, intrinsic regulation of amacrine cells' neurite growth and patterning in the developing retina although the true mechanism is likely a delicate balance between extrinsic and intrinsic cues.

Acknowledgments

We thank Colin Barnstable for providing the Vc1.1 antibody. We also thank Joyce Schiffman for expert advice on statistics.

Supported by National Institute of Neurological Disorders and Stroke R01 NS061348 (JLG); National Eye Institute R03 EY016790 (JLG), P30s EY022589 (University of California–San Diego), and EY014081 (University of Miami); National Institute of Health T32 NS007044 (MVA); The Glaucoma Foundation (JLG); a Lois Pope Undergraduate Fellowship (KTW); and an unrestricted grant from Research to Prevent Blindness.

Disclosure: **N.J. Kunzevitzky**, None; **K.T. Willeford**, None; **W.J. Feuer**, None; **M.V. Almeida**, None; **J.L. Goldberg**, None

References

1. Masland RH. Neuronal diversity in the retina. *Curr Opin Neurobiol*. 2001;11:431–436.
2. Kolb H, Nelson R, Mariani A. Amacrine cells, bipolar cells and ganglion cells of the cat retina: a Golgi study. *Vision Res*. 1981; 21:1081–1114.
3. MacNeil MA, Heussy JK, Dacheux RF, Raviola E, Masland RH. The shapes and numbers of amacrine cells: matching of photofilled with Golgi-stained cells in the rabbit retina and comparison with other mammalian species. *J Comp Neurol*. 1999;413:305–326.
4. Godinho L, Mumm JS, Williams PR, et al. Targeting of amacrine cell neurites to appropriate synaptic laminae in the developing zebrafish retina. *Development*. 2005;132:5069–5079.
5. Kay JN, Roeser T, Mumm JS, et al. Transient requirement for ganglion cells during assembly of retinal synaptic layers. *Development*. 2004;131:1331–1342.
6. Lohmann C, Myhr KL, Wong RO. Transmitter-evoked local calcium release stabilizes developing dendrites. *Nature*. 2002; 418:177–181.
7. MacNeil MA, Masland RH. Extreme diversity among amacrine cells: implications for function. *Neuron*. 1998;20:971–982.
8. Goldberg JL, Klassen MP, Hua Y, Barres BA. Amacrine-signaled loss of intrinsic axon growth ability by retinal ganglion cells. *Science*. 2002;296:1860–1864.
9. Meyer-Franke A, Kaplan MR, Pfrieger FW, Barres BA. Characterization of the signaling interactions that promote the

Investigative Ophthalmology & Visual Science

Downloaded from iovs.arvojournals.org on 04/15/2021

survival and growth of developing retinal ganglion cells in culture. *Neuron*. 1995;15:805–819.

10. Barres BA, Silverstein BE, Corey DP, Chun LL. Immunological, morphological, and electrophysiological variation among retinal ganglion cells purified by panning. *Neuron*. 1988;1: 791–803.
11. Kunzevitzky NJ, Almeida MV, Goldberg JL. Amacrine cell gene expression and survival signaling: differences from neighboring retinal ganglion cells. *Invest Ophthalmol Vis Sci*. 2010;51: 3800–3812.
12. Lake P, Clark EA, Khorshidi M, Sunshine GH. Production and characterization of cytotoxic Thy-1 antibody-secreting hybrid cell lines. Detection of T cell subsets. *Eur J Immunol*. 1979;9: 875–886.
13. Arimatsu Y, Naegele JR, Barnstable CJ. Molecular markers of neuronal subpopulations in layers 4, 5, and 6 of cat primary visual cortex. *J Neurosci*. 1987;7:1250–1263.
14. Chen Y, Stevens B, Chang J, Milbrandt J, Barres BA, Hell JW. NS21: re-defined and modified supplement B27 for neuronal cultures. *J Neurosci Methods*. 2008;171:239–247.
15. Redburn DA, Rowe-Rendleman C. Developmental neurotransmitters. Signals for shaping neuronal circuitry. *Invest Ophthalmol Vis Sci*. 1996;37:1479–1482.
16. Kong YC, Fung SC, Lam DM. Postnatal development of glycinergic neurons in the rabbit retina. *J Comp Neurol*. 1980;193:1127–1135.
17. Lam DM, Fung SC, Kong YC. Postnatal development of dopaminergic neurons in the rabbit retina. *J Neurosci*. 1981; 1:1117–1132.
18. Fung SC, Kong YC, Lam DM. Prenatal development of gabaergic, glycinergic, and dopaminergic neurons in the rabbit retina. *J Neurosci*. 1982;2:1623–1632.
19. Parkinson D, Rando RR. Ontogenesis of dopaminergic neurons in the post-natal rabbit retina: pre- and post-synaptic elements. *Brain Res*. 1984;315:207–217.
20. Lin B, Masland RH. Populations of wide-field amacrine cells in the mouse retina. *J Comp Neurol*. 2006;499:797–809.
21. Dacey DM. Axon-bearing amacrine cells of the macaque monkey retina. *J Comp Neurol*. 1989;284:275–293.
22. Dacey DM. The dopaminergic amacrine cell. *J Comp Neurol*. 1990;301:461–489.
23. Casini G, Rickman DW, Brecha NC. AII amacrine cell population in the rabbit retina: identification by parvalbumin immunoreactivity. *J Comp Neurol*. 1995;356:132–142.
24. Famiglietti EV Jr, Kolb H. A bistratified amacrine cell and synaptic circuitry in the inner plexiform layer of the retina. *Brain Res*. 1975;84:293–300.
25. Nelson R. AII amacrine cells quicken time course of rod signals in the cat retina. *J Neurophysiol*. 1982;47:928–947.
26. Brecha NC, Oyster CW, Takahashi ES. Identification and characterization of tyrosine hydroxylase immunoreactive amacrine cells. *Invest Ophthalmol Vis Sci*. 1984;25:66–70.
27. Casini G, Brecha NC. Postnatal development of tyrosine hydroxylase immunoreactive amacrine cells in the rabbit retina: I. Morphological characterization. *J Comp Neurol*. 1992;326:283–301.
28. Mariani AP. Amacrine cells of the rhesus monkey retina. *J Comp Neurol*. 1990;301:382–400.
29. Menger N, Pow DV, Wassle H. Glycinergic amacrine cells of the rat retina. *J Comp Neurol*. 1998;401:34–46.
30. Nelson R, Kolb H, Robinson MM, Mariani AP. Neural circuitry of the cat retina: cone pathways to ganglion cells. *Vision Res*. 1981;21:1527–1536.
31. Jeon CJ, Strettoi E, Masland RH. The major cell populations of the mouse retina. *J Neurosci*. 1998;18:8936–8946.
32. Turner DL, Snyder EY, Cepko CL. Lineage-independent determination of cell type in the embryonic mouse retina. *Neuron*. 1990;4:833–845.
33. Holt CE, Bertsch TW, Ellis HM, Harris WA. Cellular determination in the Xenopus retina is independent of lineage and birth date. *Neuron*. 1988;1:15–26.
34. Cepko CL, Austin CP, Yang X, Alexiades M, Ezzeddine D. Cell fate determination in the vertebrate retina. *Proc Natl Acad Sci U S A*. 1996;93:589–595.
35. Evans JA, Battelle BA. Histogenesis of dopamine-containing neurons in the rat retina. *Exp Eye Res*. 1987;44:407–414.
36. Zhang DR, Yeh HH. Histogenesis of corticotropin releasing factor-like immunoreactive amacrine cells in the rat retina. *Brain Res Dev Brain Res*. 1990;53:194–199.
37. Reese BE, Colello RJ. Neurogenesis in the retinal ganglion cell layer of the rat. *Neuroscience*. 1992;46:419–429.
38. Lee MY, Shin SL, Han SH, Chun MH. The birthdates of GABA-immunoreactive amacrine cells in the rat retina. *Exp Brain Res*. 1999;128:309–314.
39. Goldberg JL, Barres BA. The relationship between neuronal survival and regeneration. *Annu Rev Neurosci*. 2000;23:579–612.
40. Goldberg JL, Espinosa JS, Xu Y, Davidson N, Kovacs GT, Barres BA. Retinal ganglion cells do not extend axons by default: promotion by neurotrophic signaling and electrical activity. *Neuron*. 2002;33:689–702.
41. Samsonovich AV, Ascoli GA. Morphological homeostasis in cortical dendrites. *Proc Natl Acad Sci U S A*. 2006;103:1569–1574.
42. Goldberg JL. How does an axon grow? *Genes Dev*. 2003;17: 941–958.
43. Kolb H, Cuenca N, Wang HH, Dekorver L. The synaptic organization of the dopaminergic amacrine cell in the cat retina. *J Neurocytol*. 1990;19:343–366.
44. Gustincich S, Feigenspan A, Wu DK, Koopman LJ, Raviola E. Control of dopamine release in the retina: a transgenic approach to neural networks. *Neuron*. 1997;18:723–736.
45. Mariani AP, Hokoc JN. Two types of tyrosine hydroxylase-immunoreactive amacrine cell in the rhesus monkey retina. *J Comp Neurol*. 1988;276:81–91.
46. Pourcho RG, Goebel DJ. A combined Golgi and autoradiographic study of (3H)glycine-accumulating amacrine cells in the cat retina. *J Comp Neurol*. 1985;233:473–480.
47. Wassle H, Grunert U, Rohrenbeck J. Immunocytochemical staining of AII-amacrine cells in the rat retina with antibodies against parvalbumin. *J Comp Neurol*. 1993;332:407–420.
48. Casini G, Rickman DW, Trasarti L, Brecha NC. Postnatal development of parvalbumin immunoreactive amacrine cells in the rabbit retina. *Brain Res Dev Brain Res*. 1998;111:107–117.
49. Kador KE, Montero RB, Venugopalan P, et al. Tissue engineering the retinal ganglion cell nerve fiber layer. *Biomaterials*. 2013;34:4242–4250.
50. Haverkamp S, Inta D, Monyer H, Wassle H. Expression analysis of green fluorescent protein in retinal neurons of four transgenic mouse lines. *Neuroscience*. 2009;160:126–139.
51. Hertz J, Robinson R, Valenzuela DA, Lavik EB, Goldberg JL. A tunable synthetic hydrogel system for culture of retinal ganglion cells and amacrine cells. *Acta Biomater*. 2013;9: 7622–7629.

Investigative Ophthalmology & Visual Science

Downloaded from iovs.arvojournals.org on 04/15/2021